Role of FDG-PET/MRI, FDG-PET/CT, and Dynamic Susceptibility Contrast Perfusion MRI in Differentiating Radiation Necrosis from Tumor Recurrence in Glioblastomas

Mojgan Hojjati, Chaitra Badve, Vasant Garg, Curtis Tatsuoka, Lisa Rogers, Andrew Sloan, Peter Faulhaber, Pablo R. Ros, Leo J. Wolansky

From the Department of Radiology, University Hospitals Cleveland Medical Center, Cleveland, OH (MH, CB, VG, PF, PRR); Department of Neurology (Epidemiology), Case Western Reserve University, Cleveland, OH (CT); Department of Neurology, Neuro-oncology Program, University Hospitals Cleveland Medical Center, Cleveland, OH (LR); Department of Neurosurgery, University Hospitals Cleveland Medical Center, Cleveland, OH (AS); and Department of Diagnostic Imaging, University of Connecticut School of Medicine, Farmington, CT (LJW).

ABSTRACT

BACKGROUND AND PURPOSE: To compare the utility of quantitative PET/MRI, dynamic susceptibility contrast (DSC) perfusion MRI (pMRI), and PET/CT in differentiating radiation necrosis (RN) from tumor recurrence (TR) in patients with treated glioblastoma multiforme (GBM).

METHODS: The study included 24 patients with GBM treated with surgery, radiotherapy, and temozolomide who presented with progression on imaging follow-up. All patients underwent PET/MRI and pMRI during a single examination. Additionally, 19 of 24 patients underwent PET/CT on the same day. Diagnosis was established by pathology in 17 of 24 and by clinical/radiologic consensus in 7 of 24. For the quantitative PET/MRI and PET/CT analysis, a region of interest (ROI) was drawn around each lesion and within the contralateral white matter. Lesion to contralateral white matter ratios for relative maximum, mean, and median were calculated. For pMRI, lesion ROI was drawn on the cerebral blood volume (CBV) maps and histogram metrics were calculated. Diagnostic performance for each metric was assessed using receiver operating characteristic curve analysis and area under curve (AUC) was calculated.

RESULTS: In 24 patients, 28 lesions were identified. For PET/MRI, relative mean $\geq$ 1.31 resulted in AUC of .94 with both sensitivity and negative predictive values (NPVs) of 100%. For pMRI, CBV max $\geq$3.32 yielded an AUC of .94 with both sensitivity and NPV measuring 100%. The joint model utilizing r-mean (PET/MRI) and CBV mode (pMRI) resulted in AUC of 1.0.

CONCLUSION: Our study demonstrates that quantitative PET/MRI parameters in combination with DSC pMRI provide the best diagnostic utility in distinguishing RN from TR in treated GBMs.

Keywords: Glioblastoma, TR, RN, PET/MRI, DSC-pMRI.

Acceptance: Received March 2, 2017, and in revised form June 24, 2017. Accepted for publication June 26, 2017.

Correspondence: Address correspondence to Chaitra Badve, MD, Department of Radiology, University Hospitals Cleveland Medical Center, Cleveland, OH 44106, USA. E-mail: chaitra.badve@uhhospitals.org.

Acknowledgments and Disclosure: The current manuscript has not received financial grant support. Author Mojgan Hojjati was funded by a research grant from Philips Healthcare, manufacturers of the PET-MRI system used to scan the patients described. None of the remaining authors have potential conflicts of interest.

J Neuroimaging 2018;28:118-125.
DOI: 10.1111/jon.12460

Introduction

Glioblastomas represent 15.1% of all primary brain tumors and 55.1% of all gliomas with an incidence of two to three cases per 100,000 people.[1,2] The current standard of care therapy for high-grade gliomas consists of maximum safe surgical resection followed by radiotherapy and concomitant/adjuvant temozolomide chemotherapy. Up to 30% of patients develop treatment-related injury that can mimic tumor recurrence (TR) by conventional MRI.[3,4] The overlapping imaging features pose a diagnostic dilemma requiring follow-up imaging or invasive biopsy, which can cause a delay in diagnosis or unnecessary morbidity, respectively.[5] It is critical for optimum patient management to determine in a timely manner if imaging progression represents TR or radiation necrosis (RN).

The incidence of RN after radiotherapy for cerebral neoplasms ranges from 3% to 24%.[6] The likelihood of RN is related to both the volume of irradiated brain and the total radiation dose administered and the administration of chemotherapy. With a total dose of <45 Gy, 5% of patients may develop necrosis,[7] whereas the likelihood of necrosis markedly increases with a total dose of >64.8 Gy.[8] The exact pathogenesis of radiation-induced toxicity is not fully understood but includes a combination of the following proposed mechanisms: vascular injury, glial and white matter damage, and alterations in the fibrinolytic enzyme and immune systems.[9] Radiation therapy (RT) and chemotherapy can alter the blood-brain barrier, leading to increased vascular permeability and increased contrast enhancement even in the absence of tumor.[10,11]

Several advanced imaging techniques have been used to discriminate between RN and TR including perfusion imaging, permeability imaging, MR spectroscopy, and PET imaging (with ^{18}F-Fluoro-deoxy-glucose FDG and non-FDG

tracers).[12–15] These techniques have shown varying abilities to differentiate between RN and TR; however, most of these studies have evaluated the role of only one advanced imaging technique at a time. Currently, there is no consensus regarding which technique or combinations of techniques have the best ability to address this diagnostic challenge.

In our study, we compared the efficacy of quantitative ^{18}F-FDG PET/MRI, ^{18}F-FDG PET/CT, and dynamic susceptibility contrast (DSC) perfusion MRI (pMRI) in evaluating imaging progression in post therapy glioblastoma multiforme (GBM) to differentiate between TR and RN. We sought to examine the diagnostic performance of these three modalities separately as well as via a multiparametric joint model approach.

Materials and Methods

Ethical Approval

This HIPAA-compliant (Health Insurance Portability and Accountability) study was approved by the institutional review board at University Hospitals Cleveland Medical Center in Cleveland, Ohio. All subjects received both oral and written information regarding the study and signed an informed consent prior to participation.

Patient Population

The inclusion criteria were patients with GBM treated with surgery, radiation, and concomitant/adjuvant temozolomide chemotherapy, who subsequently presented with new and/or increasing enhancement around the resection site on follow-up MR imaging (ie, imaging progression). This retrospective study took place in 2013-2014 and included 24 patients with 28 lesions with a male to female ratio of 16:8, age range of 34-81 years, and a mean age of 57.5 years. All lesions had previously been treated with partial brain RT (mean dose of 58.62 Gy). The median time elapsed between the end of radiation treatment and the appearance of a new lesion was 19 months (range 2-90 months).

Lesion Diagnosis

Advanced imaging was performed to further characterize imaging progression and to differentiate between RN and TR. Patients with imaging and clinical characteristics concerning for TR subsequently underwent a surgical biopsy or resection. On pathology, RN was defined as the presence of treatment-related tissue effects with less than 20% viable tumor in the pathologic specimen; whereas the presence of more than 20% viable tumor was defined as TR. Patients with clinical and imaging characteristics suggestive of RN or patients unfit for surgical intervention underwent clinical and imaging follow up. Following this rationale, the final diagnosis was confirmed by histopathology in 17 of the 24 patients. In the remaining seven cases, the final diagnosis was established by clinical and imaging stability on follow-up (follow-up ranging from 8 to 18 months). These seven patients were clinically followed for a range of 134-395 days after completion of RT. A flowchart of the number of patients screened can be found in Figure 1.

Imaging Protocol

All patients underwent ^{18}F-FDG PET/MRI (with MR attenuation correction, MRAC) and pMRI in a single examination using a 3 Tesla Philips Ingenuity TF PET/MRI system (Philips Healthcare, Andover, MA, USA). Of these 24 patients, 19 patients concurrently underwent ^{18}F-FDG PET/CT on the same day (single FDG dose) prior to undergoing the PET/MRI study. The median scan delay between the two modalities was 10-15 minutes. The PET/CT scanners and PET/MRI scanner were located in the suite approximately 60 meters apart. The total scan time including both the PET/CT and PET/MRI imaging was 110 minutes. The average scan time of the PET/MRI alone was 90 minutes. The workflow and imaging protocol is illustrated in Figure 2.

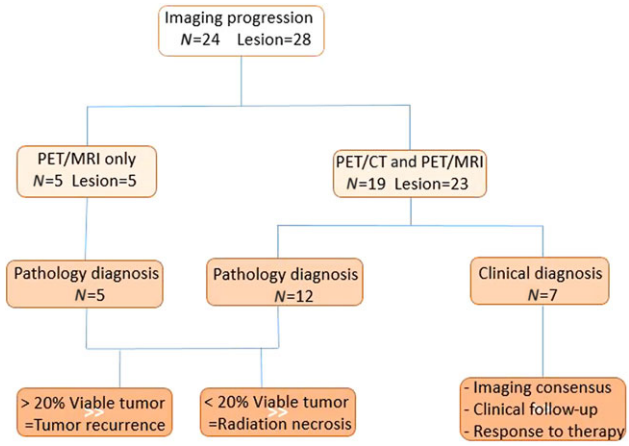

Fig 1. Flow diagram illustrating the number of patients (*N*) and total lesions screened.

PET/CT Acquisition

The PET/CT scanning of the brain was performed on a Gemini TF PET/CT scanner (Philips Healthcare). Each of the patients fasted for at least 6 hours prior to the ^{18}F-FDG administration. A median dose of 4.44×10^8 Becquerels (Bq) ^{18}F-FDG (range $3.33\text{-}5.55 \times 10^8$ Bq) was administered via a cubital vein catheter. To reduce brain stimulation and tracer uptake within the cortex, the patients rested silently in the dark and in a warm atmosphere from 15 minutes prior to the injection until 30 minutes after the injection. The standard of care post injection delay was used for the PET/CT. The uptake time between the tracer injection and PET scan was approximately 45 minutes. The PET data were acquired in 10 minutes at one bed position. The CT parameters were 120 kVp, 50 mAs, and a slice thickness of 5 mm.

PET/MRI Acquisition

The PET/MRI examination was performed on a sequential PET/MRI scanner system (Ingenuity TF PET/MRI, Philips Healthcare).[16,17] The PET acquisition parameters were identical for the PET/CT and PET/MRI imaging. The PET/MRI examination was performed after PET/CT in 19 subjects and after an ^{18}F-FDG uptake of approximately 57 minutes. For the remaining five patients who only underwent PET/MRI, a protocol similar to the aforementioned PET/CT protocol was followed. A 3-dimensionalmultistation spoiled gradient echo attenuation MR of the brain preceded the PET scanning to obtain attenuation correction information for the PET data.[17] Acquisition time was 10 minutes for one bed position. The PET/MRI acquisition preceded the diagnostic MRI scan.

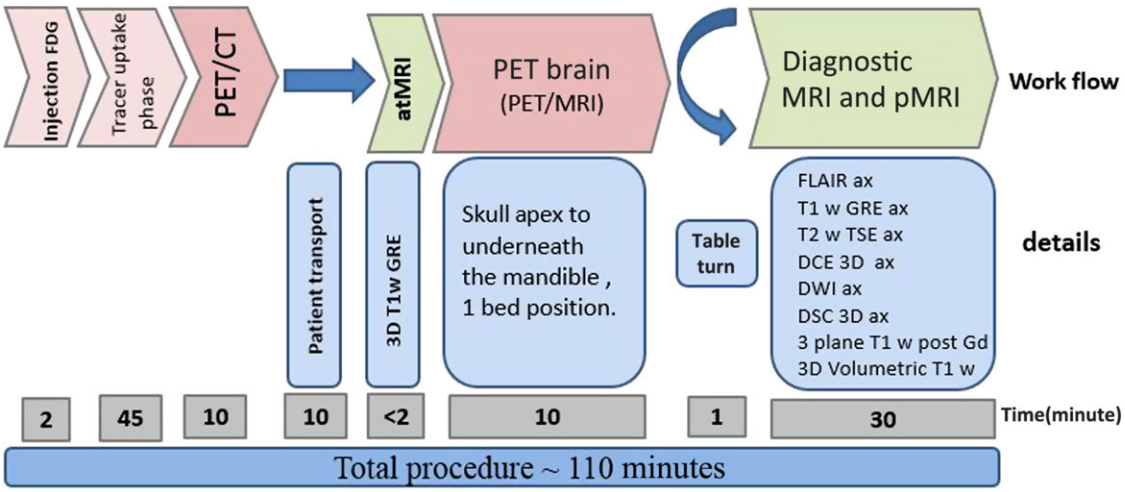

Fig 2. Workflow for PET/CT and combined PET/MRI of the brain for evaluation of imaging progression in post therapy glioblastoma patients. FDG = fludeoxyglucose; atMRI = attenuation MRI; pMRI = perfusion MRI; 3D = 3 dimensional; T1w = T1 weighted; GRE = gradient recalled echo; FLAIR = fluid-attenuated inversion recovery; ax = axial; T2w = T2 weighted; TSE = turbo spin echo; DCE = dynamic contrast-enhanced; DWI = diffusion-weighted imaging; DSC = dynamic susceptibility contrast; Gd = gadolinium; min = minute.

Diagnostic MR Imaging

In addition to the DSC parameters described below, standard MRI sequences included axial FLAIR, axial T1 GRE, axial T2 TSE, and axial diffusion-weighted imaging (DWI) with apparent diffusion coefficient (ADC) maps were obtained.

DSC

Initial dynamic contrast enhancement (DCE) MRI was obtained during rapid administration of 5 mL Gadoversetamide (Optimark, Mallinckrodt Inc., St. Louis, MO, USA) for permeability imaging. Preacquisition of DCE MRI provided a preloading dose of contrast to reduce errors from leakage during DSC calculations.

After a 5-7 minute delay, DSC perfusion imaging was acquired during rapid infusion of 15 mL Gadoversetamide using dynamic T2*-weighted gradient-echo echo-planar imaging pulse sequence. The contrast agent bolus was power-injected though a peripheral intravenous catheter at 2-5 mL/second and immediately followed by a 20-mL saline flush at the same rate.

Imaging parameters were as follows: TR = 14 ms, TE = 21 ms, FOV = 230 × 230 mm², matrix = 160 × 160 voxel, in-plane voxel size 3.5 × 3.5 × 5 mm, FA = 7°, 16 slices, slice thickness 5 mm, and temporal resolution 1.5 seconds without acceleration factor. The total acquisition time of the DSC sequence was 3 minutes and 27 seconds. Postprocessing of DSC imaging was performed at a dedicated workstation utilizing FDA-approved (Food and Drug Administration) Olea Sphere 2.2 software (Olea Medical Solutions, La Ciotat, France) by a board-certified radiologist. The cerebral blood volume (CBV) was estimated on a voxel basis after a post bolus baseline correction by mathematical integration of the area under the curve in each voxel.

Image Reconstruction and Analysis

PET/CT and PET/MRI images were analyzed on an MIM workstation (MIM version 6.1 Software™, Cleveland, OH, USA). For quantitative PET/CT analysis, a fellowship-trained neuroradiologist analyzed the data as follows: The PET/CT and contrast enhanced T1 images were imported together in MIM and an image coregistration was performed using intracranial and extracranial anatomical landmarks. Once the coregistration was deemed to be satisfactory, a region of interest (ROI) was drawn around the lesion (L) on the PET attenuation corrected map using the contrast enhanced T1 images as the underlay. The PET edge detection tool was used for drawing the ROI, which was then manually checked and corrected for further accuracy. Similarly, another ROI was placed on the contralateral healthy white matter (C). These ROIs were saved as separate files and maximum, mean, and median standard uptake values (SUV; defined as tissue concentration [MBq/g] × body weight [g])/(injected dose [MBq]) for each ROI were recorded. Similar methodology was followed for the subset of patients who underwent only PET/MRI scan ($n = 5$).

In patients who underwent PET/CT and PET/MRI scans, quantitative PET/MRI analysis was performed as follows. As the first step, image coregistration was performed using PET/CT, PET/MRI, and contrast enhanced T1-weighted images. Then, the PET/CT ROI tracings were copied and coregistered on MR attenuation-corrected PET images (MRAC PET) by a board-certified radiologist also while using contrast enhanced T1 images as an underlay.

DSC perfusion analysis was performed on the MIM workstation by a board-certified radiologist. Using PET ROIs described above as references, new ROIs were drawn on quantitative CBV maps using contrast enhanced T1 images as an underlay. Areas of hemorrhage, blood vessels, susceptibility artifacts, and cystic or necrotic change were excluded. Quantitative CBV values for each pixel within the ROI were recorded and histogram metrics were calculated. Figure 3 demonstrates an example of an ROI analysis on an MIM workstation.

Statistical Analysis

For PET/MRI and PET/CT, the lesion to contralateral white matter (L/C) ratios were computed using respective mean, median, and maximum SUV values from target ROIs. For pMRI, in addition to mean, median, maximum, and mode CBV values

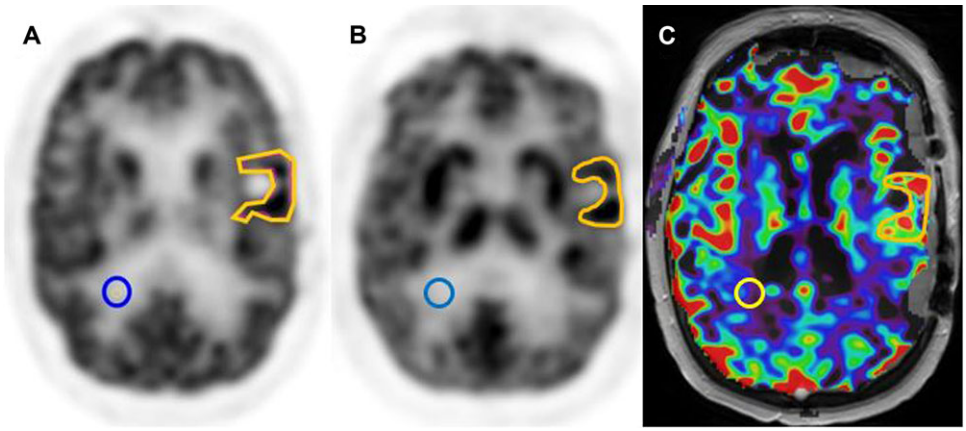

Fig 3. Quantitative PET/CT and PET/MRI region of interest (ROI) analyses were performed on computed tomography attenuation correction PET (A) and magnetic resonance attenuation correction PET (B) images using MIM software. Quantitative dynamic susceptibility contrast perfusion MRI ROI analysis was performed on cerebral blood volume maps (C).

from each ROI, the following parameters were computed: skewness, kurtosis, 25th, 75th, and 90th percentile, and standard deviation of CBV voxel values within an ROI. The diagnostic accuracy of all these parameters was assessed using receiver operating characteristic (ROC) curve analysis, with recurrent tumor defined as more than 20% viable tumor in the pathologic specimen and considered as the "positive" outcome in analyses. Cutoff values were selected based on balancing the specificity and sensitivity values, minimizing the maximum value between false positive and false negative rates.

Multivariate logistic regression model was used to assess the performance of pMRI with PET/MRI, where explanatory variables were selected based on maximizing AUC values within a respective modality. Using this model, a probability of being a recurrent tumor was estimated for each case. These estimated probability values were considered as diagnostic variables and were further used for ROC curve analysis.

Results

PET/MRI and DSC pMRI were performed in all patients (24 patients and 28 lesions) and PET/CT was available for 19 of the patients (23 lesions). The DSC pMRI data were excluded for one patient due to errors in data processing. Of the 24 patients and 28 lesions, 22 lesions were diagnosed as true recurrent tumors and 6 lesions as RN. Figures 4 and 5 are two case examples, which demonstrate the diagnostic utility of PET/MRI and pMRI in differentiating recurrent tumor (Fig 4) from tumor necrosis (Fig 5).

Quantitative Analysis and Diagnostic Performance of PET/MRI and PET/CT (Paired Analysis N = 23 Lesions)

Among the quantitative PET/MRI metrics, r-mean values ≥ 1.31 were most effective in differentiating TR from RN yielding a sensitivity of 100%, specificity of 80%, NPV = 100%, positive predictive value (PPV) = 94.7%, and AUC of .94.

Among the quantitative PET/CT metrics, r-mean values ≥ 1.47 performed best and yielded a sensitivity of 83%, specificity of 80%, NPV = 57.1%, PPV = 93.8%, and AUC of .89. The diagnostic performance of the quantitative PET/MRI and PET/CT metrics is summarized in Table 1.

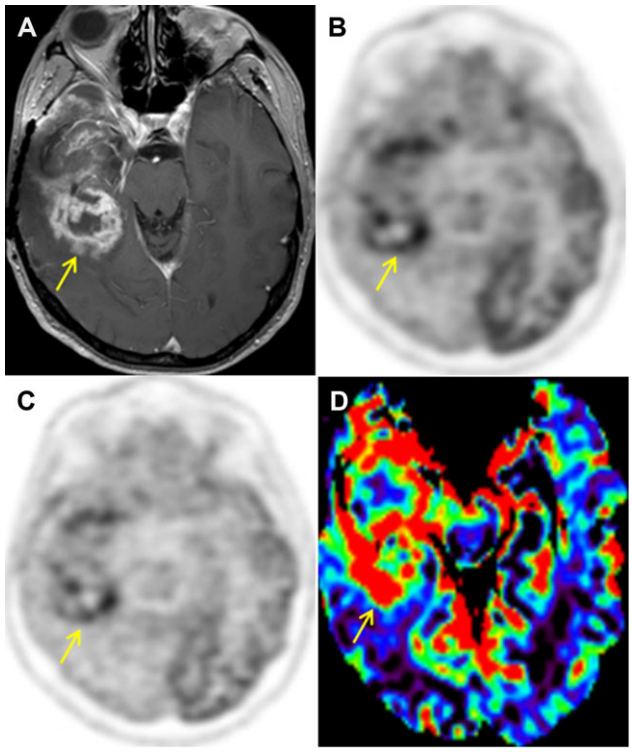

Fig 4. A 54-year-old male with right temporal glioblastoma multiforme status post standard therapy with complex history of prior imaging progression and resections presented with new imaging progression 15 months after most recent radiation therapy. Axial post contrast T1 (A), computed tomography attenuation correction PET (B), magnetic resonance attenuation correction PET (C), and cerebral blood volume (CBV) map (D) demonstrate increased fludeoxyglucose uptake and increased CBV within the peripheral (enhancing) portion of the lesion (arrows). Pathology revealed viable glioma comprising > 50% of the resection specimen.

Quantitative Analysis and Diagnostic Performance of DSC MRI

The logistic regression analysis revealed that four CBV histogram metrics with the highest diagnostic utility for differentiating TR from RN were mean, median, mode, and maximum.

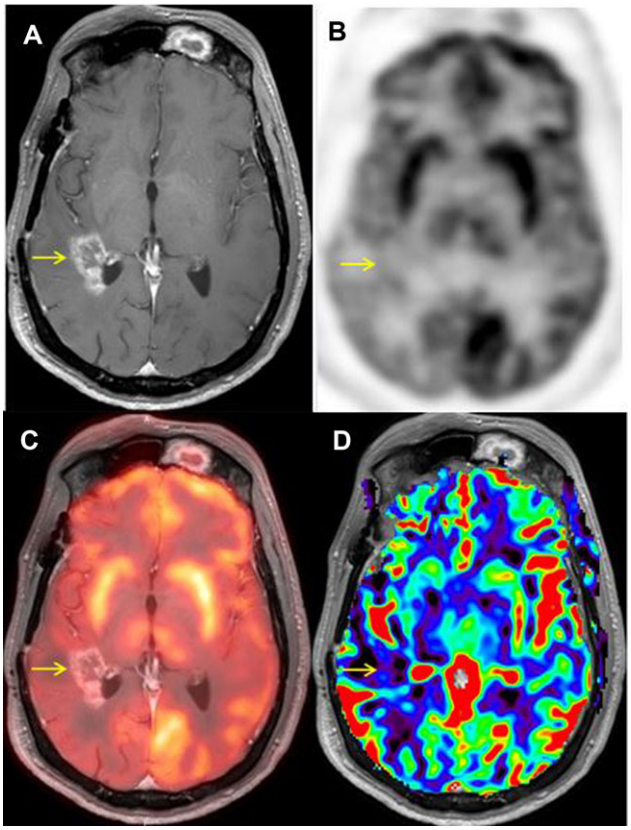

Fig 5. History of right temporal anaplastic astrocytoma World Health Organization Grade III, 18 months post treatment with recurrent enhancing right periatrial temporal lesion (arrow). Axial post contrast T1 (A), magnetic resonance attenuation correction (MRAC) PET (B), MRAC PET with T1 underlay (C), and cerebral blood volume (CBV) map with T1 underlay (D) demonstrate no significant increased lesional CBV or fludeoxyglucose (FDG) uptake. Fused image (C) demonstrates faint FDG uptake due to "Contrast enhanced MRI-underlay image shine-through." Pathology revealed radiation necrosis.

Remainder of the histogram parameters were not significant and were not tested any further. CBV max ≥3.32 performed the best with a sensitivity of 100%, specificity of 75%, NPV = 100%, PPV = 94.7%, and AUC of .94. The diagnostic performance of the significant CBV histogram metrics is outlined in Table 2.

Combined Model DSC MRI and PET/MRI

Joint model statistical analysis was performed to evaluate whether the diagnostic yield of a DSC perfusion imaging improved when combined with the best performing PET/MRI parameter. The CBV mode value demonstrated higher specificity and similar AUC relative to the CBV median and mean variables. CBV mode also demonstrated higher specificity and better performance in joint modeling as compared to CBV maximum and hence was selected as the PET/MRI parameter. Therefore, the optimal joint model included r-mean for PET/MRI (based on Table 1) in combination with the CBV mode. The joint model of the PET/MRI r-mean and pMRI CBV mode with a cutoff value of .73 or above as recurrent tumor resulted in a sensitivity of 100%, specificity of 100%, NPV = 100%, PPV = 100%, and AUC of 1.0. The combination of these two parameters improved diagnostic accuracy over either one of the modalities alone. These joint model values are outlined in Table 3.

Discussion

This study quantitatively compared the diagnostic utility of PET/MRI, PET/CT, and DSC pMRI in distinguishing between RN and TR in treated GBMs and demonstrated a superior diagnostic performance of PET/MRI when compared to PET/CT. Furthermore, it showed that the combination of PET/MRI and pMRI offers the best performing diagnostic tool to accurately differentiate between the two entities.

Histopathological tissue diagnosis remains the gold standard in differentiating between RN and TR; however, this procedure is associated with potential sampling error, operative risk, and morbidity.[18] Moreover, in pathology practice, it is not easy to differentiate a recurrent GBM from therapy-related changes as a mixture of both recurrent tumor and RN remains the most common histologic presentation.[19,20] The diagnosis of recurrence can therefore be subjective and quantitative criteria for histopathological diagnosis of recurrent GBMs have been suggested.[19,21] Kim et al[22] evaluated the prognostic value of residual viable tumor volume versus therapy-induced necrosis volume in resection material of 20 patients with recurrent GBM. Their results showed prolonged survival in patients with recurrent GBM in whom the recurrent tumor volumes, including high-grade and nonhigh-grade tumor components, were <20%.[22] Hence, in our study, recurrent tumor was defined as more than 20% viable tumor in the pathologic specimen.

MRI remains the modality of choice in the diagnosis, treatment planning, and follow up of brain tumors owing to its superb soft tissue contrast and anatomical detail.[23] However, differentiation of RN and TR in treated tumors using conventional MRI is extremely difficult due to very similar imaging presentations. A systematic review by Shah et al identified three

Table 1. Diagnostic Performance of PET/CT and PET/MRI (N = 23 Lesions)

	PET/MRI r-Mean, Cutoff ≥1.31	PET/MRI r-Median, cutoff ≥1.35	PET/MRI r-Max, cutoff ≥1.90	PET/CT r-Mean, Cutoff ≥1.47	PET/CT r-Median, cutoff ≥1.48	PET/CT r-Max, Cutoff ≥1.86
N	23	23	23	23	23	23
Sensitivity	100%	94.4%	83.3%	83%	83%	77.8%
Specificity	80%	80%	100%	80%	80%	80%
NPV	100%	80%	62.5%	57.1%	57.1%	50%
PPV	94.7%	94.4%	100%	93.8%	93.8%	93.3%
AUC	.94	.92	.94	.88	.87	.85

Among the quantitative metrics of PET/CT and PET/MRI, r-mean values were most effective in differentiating tumor recurrence from radiation necrosis.
r-mean = relative mean; r-median = relative median; r-max = relative maximum; N = number; NPV = negative predictive value; PPV = positive predictive value; AUC = area under the curve.

Table 2. Diagnostic Performance of Dynamic Susceptibility Contrast (DSC) Perfusion MRI Histogram Metrics

	DSC-MRI CBV Mode Cutoff ≥3.39	DSC-MRI CBV Mean Cutoff ≥1.73	DSC-MRI CBV Median Cutoff ≥1.62	DSC-MRI CBV Maximum Cutoff ≥3.32
N	22	22	22	22
Sensitivity	77.8%	100%	100%	100%
Specificity	100%	75%	75%	75%
NPV	50%	100%	100%	100%
PPV	100%	94.7%	94.4%	94.7%
AUC	.91	.91	.91	.94

Among cerebral blood volume (CBV) histogram metrics, CBV maximum performed best in differentiating tumor recurrence from radiation necrosis.
N = number; NPV = negative predictive value; PPV = positive predictive value; AUC = area under the curve; DSC = dynamic susceptibility contrast; CBV = cerebral blood volume.

Table 3. Combined Model Dynamic Susceptibility Contrast (DSC) Perfusion MRI and PET/MRI or PET/CT

	PET/MRI r-Mean, Cutoff ≥1.31	PET/CT r-Mean, Cutoff ≥1.47	Perfusion CBV Mode Cutoff ≥ 3.39	PET/MRI r-Mean and CBV Mode Joint Model, Cutoff ≥ .73
N	23	23	22	23
Sensitivity	100%	83%	77.8%	100%
Specificity	80%	80%	100%	100%
NPV	100%	57.1%	50%	100%
PPV	94.7%	93.8%	100%	100%
AUC	.94	.88	.91	1.0

Combination of PET/MRI r-mean value with cerebral blood volume (CBV) mode improved diagnostic performance over either one of the modalities and also over PET/CT r-mean and CBV mode joint model.
N = number; NPV = negative predictive value; PPV = positive predictive value; AUC = area under the curve; r-mean = relative mean (ratio); CBV = cerebral blood volume.

studies differentiating RN and TR by conventional MRI, which reported a high sensitivity of 88.9% but poor specificity of only 33.4%.[21]

PET with or without CT attenuation allows for improved metabolic characterization of tissues with reported sensitivities and specificities for differentiation of RN versus TR ranging from 65% to 81% and 40% to 94%, respectively.[14,24–28] Earlier reports dating back to 1982 suggested highly promising clinical utility of PET in differentiating between the two entities although these results have not been reproducible in subsequent literature.[24] A more recent study raised concern for the suboptimal ability of PET/CT to differentiate RN and TR with a sensitivity and specificity of 73% and 56%, respectively, when using the contralateral gray matter as the reference standard and 22% specificity with the contralateral white matter as the reference.[27] The study determined that the physiological brain activity adjacent to and altered biomechanics secondary to the resection site as well as occasional paradoxical hypermetabolic activity seen with RN and hypometabolic activity with TR resulted in higher count of false positive and false negative examinations. Furthermore, this study hypothesized that prior studies reporting higher diagnostic yields were falsely elevated secondary to suboptimal clinical and imaging follow-up resulting in inaccurate classification of TR and RN, which in theory could have been avoided if the gold standard histopathology analysis were to be performed.

As the utility of PET imaging in management of brain tumors has gained wider recognition, there has been significant interest to evaluate the diagnostic performance of PET when combined with the optimal soft tissue contrast of MRI.[29–31] Chao et al in 2001 demonstrated the improved sensitivity of ^{18}F-FDG-PET coregistered with MRI when compared to FDG PET alone (86% vs. 65%) to distinguish RN from TR.[29] The latest hybrid PET/MRI machines allow for exact coregistration of PET and MRI data, essentially eliminating misregistration secondary to differences in head positioning and secondary to motion and therefore hold the promise to provide accurate anatomical delineation in a one-stop imaging approach.

The advanced MRI technique of pMRI allows for the characterization of tissue physiology through information regarding the integrity of blood-brain barrier, degree of neoangiogenesis, and alterations in microvascular permeability, all of which enable the detection of viable high-grade neoplasm. A review by Shah et al identified six studies evaluating the sensitivity and specificity of pMRI for TR (vs. RN) and demonstrated a cumulative sensitivity of 79.8% and specificity of 76.8%.[32] Kim et al in 2010 revealed the superior characteristics of CBV in distinguishing RN from TR in high-grade gliomas compared to ^{18}F-FDG and ^{11}C-MET PET, albeit the statistical significance could not be proven due to small number of cases.[33]

There are very few published studies that directly compare the efficacy of pMRI with metabolic imaging despite the fact that PET imaging and pMRI assess completely different aspects of tumor biology and can provide complementary information. Our results suggest that PET/MRI in combination with pMRI has the potential to be the comprehensive diagnostic tool in addressing this vexing question. The technological advances behind hybrid PET/MRI scanners allow PET, MRI, and pMRI imaging in a single visit thereby allowing for perfect imaging coregistration across modalities. Although the acquisition of PET/CT is quicker than PET/MRI, the fact that pMRI can be obtained simultaneously with PET/MRI not only provides a technical advantage which can positively affect the diagnostic yield, but may also be more time and cost efficient compared to the separate acquisition of PET/CT, MRI brain, and pMRI.

Limitations to the study must be acknowledged. Although PET/MRI was performed in each of the 23 patients, PET/CT data were available in a smaller subset of the participants. A larger prospective study must be performed to confirm the initial finding demonstrated by our study. There was a 10–15 minute delay between PET/CT and PET/MRI acquisitions which in theory could affect the lesion to background ratio, perhaps due to rapid clearance of tracer from normal brain parenchyma. Future studies with a crossover study design would address this limitation satisfactorily. The proportion of RN was lower relative to the number of patients with true recurrent tumors. A more even balance of true positives and true negatives would strengthen the statistical analysis. One of the realistic problems with imaging progression is that the target area may represent a "mixed lesion" with a combination of TR and RN. The authors assigned the cutoff of 20% viable tumor in distinguishing recurrent tumor from treatment-related changes based on a single study.[22] A future study that accounts for mixed character of imaging progression with quantitation of viable tumor estimates based on imaging features with histopathological correlation could perhaps offer a robust study design to address this problem.

Larger, prospective trials are necessary to confirm the improved diagnostic value of PET/MRI (including pMRI) over PET/CT with specifically using the qualitative cutoff values provided in this manuscript. Analysis of different radiotracers, perfusion techniques, and quantitative architectural analysis may support and fortify our ability to accurately and precisely identify RN and TR.

Conclusion

In this retrospective study, PET/MRI in combination with pMRI CBV demonstrated a 100% diagnostic sensitivity and 100% specificity in distinguishing tumor progression from RN in post treatment GBMs and outperformed all other modalities individually.

References

1. American Brain Tumor Association. Brain tumor statistics. Available at: www.abta.org/about-us/news/brain-tumor-statistics/. Accessed March 15, 2016.
2. Stevens GHJ. Brain tumors–meningiomas and gliomas. Cleveland Clinic. Available at: http://www.clevelandclinicmeded.com/medicalpubs/diseasemanagement/hematology-oncology/brain-tumors/. Accessed March 15, 2016.
3. Alexiou GA, Tsiouris S, Kyritsis AP, et al. Glioma recurrence versus radiation necrosis: accuracy of current imaging modalities. J Neurooncol 2009;95:1-11.
4. Brandes AA, Tosoni A, Spagnolli F, et al. Disease progression or pseudoprogression after concomitant radiochemotherapy treatment: pitfalls in neurooncology. Neuro Oncol 2008;10:361-7.
5. Mamlouk MD, Handwerker J, Ospina J, et al. Neuroimaging findings of the post-treatment effects of radiation and chemotherapy of malignant primary glial neoplasms. Neuroradiol J 2013;26:396-412.
6. Brandsma D, Stalpers L, Taal W, et al. Clinical features, mechanisms, and management of pseudoprogression in malignant gliomas. Lancet Oncol 2008;9:453-61.
7. Marks JE, Baglan RJ, Prassad SC, et al. Cerebral radionecrosis: incidence and risk in relation to dose, time, fractionation and volume. Int J Radiat Oncol Biol Phys 1981;7:243-52.
8. Leibel SA, Sheline GE. Radiation therapy for neoplasms of the brain. J Neurosurg 1987;66:1-22.
9. Kumar AJ, Leeds NE, Fuller GN, et al. Malignant gliomas: MR imaging spectrum of radiation therapy- and chemotherapy-induced necrosis of the brain after treatment. Radiology 2000;217:377-84.
10. Hygino da Cruz LC, Jr., Rodriguez I, Domingues RC, et al. Pseudoprogression and pseudoresponse: imaging challenges in the assessment of posttreatment glioma. AJNR Am J Neuroradiol 2011;32:1978-85.
11. Brandes AA, Franceschi E, Tosoni A, et al. MGMT promoter methylation status can predict the incidence and outcome of pseudoprogression after concomitant radiochemotherapy in newly diagnosed glioblastoma patients. J Clin Oncol 2008;26:2192-7.
12. Spaeth N, Wyss MT, Weber B, et al. Uptake of 18F-fluorocholine, 18F-fluoroethyl-L-tyrosine, and 18F-FDG in acute cerebral radiation injury in the rat: implications for separation of radiation necrosis from tumor recurrence. JNM J Nucl Med 2004;45:1931-8.
13. Sugahara T, Korogi Y, Tomiguchi S, et al. Posttherapeutic intraaxial brain tumor: the value of perfusion-sensitive contrast-enhanced MR imaging for differentiating tumor recurrence from nonneoplastic contrast-enhancing tissue. AJNR Am J Neuroradiol 2000;21:901-9.
14. Kim YH, Oh SW, Lim YJ, et al. Differentiating radiation necrosis from tumor recurrence in high-grade gliomas: assessing the efficacy of 18F-FDG PET, 11C-methionine PET and perfusion MRI. Clin Neurol Neurosurg 2010;112:758-65.
15. Schlemmer H-P, Bachert P, Henze M, et al. Differentiation of radiation necrosis from tumor progression using proton magnetic resonance spectroscopy. Neuroradiology 2002;44:216-22.
16. Zaidi H, Ojha N, Morich M, et al. Design and performance evaluation of a whole-body Ingenuity TF PET-MRI system. Phys Med Biol 2011;56:3091-106.
17. Kalemis A, Delattre BM, Heinzer S. Sequential whole-body PET/MR scanner: concept, clinical use, and optimisation after two years in the clinic. The manufacturer's perspective. Magn Reson Mater Phys Biol Med 2013;26:5-23.
18. Srinivasan R, Phillips JJ, Vandenberg SR, et al. Ex vivo MR spectroscopic measure differentiates tumor from treatment effects in GBM. Neuro Oncol 2010;12:1152-61.
19. Perry A, Schmidt RE. Cancer therapy-associated CNS neuropathology: an update and review of the literature. Acta Neuropathol 2006;111:197-212.
20. Tihan T, Barletta J, Parney I, et al. Prognostic value of detecting recurrent glioblastoma multiforme in surgical specimens from patients after radiotherapy: should pathology evaluation alter treatment decisions? Hum Pathol 2006;37:272-82.
21. Shah AH, Snelling B, Bregy A, et al. Discriminating radiation necrosis from tumor progression in gliomas: a systematic review what is the best imaging modality? J Neurooncol 2013;112:141-52.
22. Kim JH, Bae Kim Y, Han JH, et al. Pathologic diagnosis of recurrent glioblastoma: morphologic, immunohistochemical, and molecular analysis of 20 paired cases. Am J Surg Pathol 2012;36:620-8.
23. Essig M, Weber M-A, von Tengg-Kobligk H, et al. Contrast-enhanced magnetic resonance imaging of central nervous system tumors: agents, mechanisms, and applications. TMRI Top Magn Reson Imaging 2006;17:89-106.
24. Patronas N, Di Chiro G, Brooks R, et al. Work in progress: [18F] fluorodeoxyglucose and positron emission tomography in the evaluation of radiation necrosis of the brain. Radiology 1982;144:885-9.
25. Kim E, Chung S, Haynie T, et al. Differentiation of residual or recurrent tumors from post-treatment changes with F-18 FDG PET. Radiographics 1992;12:269-79.
26. Kahn D, Follett K, Bushnell D, et al. Diagnosis of recurrent brain tumor: value of 201Tl SPECT vs 18F-fluorodeoxyglucose PET. AJR Am J Roentgenol 1994;163:1459-65.
27. Ricci PE, Karis JP, Heiserman JE, et al. Differentiating recurrent tumor from radiation necrosis: time for re-evaluation of positron emission tomography? AJNR Am J Neuroradiol 1998;19:407-13.
28. Langleben DD, Segall GM. PET in differentiation of recurrent brain tumor from radiation injury. J Nucl Med 2000;41:1861-7.
29. Chao ST, Suh JH, Raja S, et al. The sensitivity and specificity of FDG PET in distinguishing recurrent brain tumor from

radionecrosis in patients treated with stereotactic radiosurgery. Int J Cancer 2001;96:191-7.
30. Wong TZ, van der Westhuizen GJ, Coleman RE. Positron emission tomography imaging of brain tumors. Neuroimaging Clin N Am 2002;12:615-26.
31. Hustinx R, Pourdehnad M, Kaschten B, et al. PET imaging for differentiating recurrent brain tumor from radiation necrosis. Radiol Clin North Am 2005;43:35-47.
32. Shah R, Vattoth S, Jacob R, et al. Radiation necrosis in the brain: imaging features and differentiation from tumor recurrence. Radiographics 2012;32:1343-59.
33. Kim YH, Oh SW, Lim YJ, et al. Differentiating radiation necrosis from tumor recurrence in high-grade gliomas: assessing the efficacy of 18 F-FDG PET, 11 C-methionine PET and perfusion MRI. Clin Neurol Neurosurg 2010;112:758-65.